



Lamination curing method for silver nanoparticle inkjet printed flexible electronics: design, uncertainty and performance analysis

Dila Türkmen¹ , and Merve Acer Kalafat^{1,*}

¹ Mechanical Engineering Department, Istanbul Technical University, Istanbul, Turkey

Received: 17 April 2023

Accepted: 26 August 2023

Published online:
5 October 2023

© The Author(s), under exclusive licence to Springer Science+Business Media, LLC, part of Springer Nature, 2023

ABSTRACT

In this paper, we propose a fast, simple, low-cost and high-performance curing method, “lamination curing”, to activate silver nano-particle inkjet printed flexible electronics, as a new and advantageous alternative to the existing curing methods. Proposed method is tested together with the most widely-used method in the literature (oven curing), and provided a lower sheet resistance and fabrication uncertainty. The method provided a major advantage of curing the low thermal resistant substrates at higher temperatures without distortion and under 3 min (~2 mm/s). Microstructure images approved the lamination curing provided a better aggregation, matching with the higher conductivity. Effects of different curing parameters on the resulting conductivity and uncertainty are analysed for both methods. Finally, printed patterns are applied and tested as angle sensors, and found to have more consistent angle sensing behaviors with higher overall sensing performance when lamination cured. We state lamination curing as an advantageous and reliable alternative to oven curing and other fast curing methods both for sensor and circuitry printing implementations.

1 Introduction

Inkjet printing is the most preferred method for the flexible electronics, especially in R&D applications [1]. Silver nanoparticle (Ag NP) inks are one of the widest used materials both for the passive and active circuit elements [2–6]. Despite the relatively simple and fast printing process provided by the inkjet method, Ag NP inks require post-printing curing processes to become electrically conductive, as the ink solutions contain non-conductive compounds (stabilizers) to

facilitate printing, which avoid conductive particles to contact each other [7]. Sufficient percolation through the conductive particles needs to be reached for high conductivity and stable performances of the printed elements [8].

Table 1 lists the reported curing methods in the literature [7, 9, 10], in terms of their performances in conductivity, curing speed, resulting film and substrate quality, financial and technical cost, and compatibility with R2R (roll-to-roll) processes. While none of the existing methods provide sufficient solutions in all of

Address correspondence to E-mail: acerm@itu.edu.tr

E-mail Addresses: turkmend@itu.edu.tr

Table 1 Advances (green) and open problems (red) in curing methods for inkjet printed nanoparticle films

Method	Conductivity	Speed	Film quality	Substrate quality	Cost	Compatibility with R2R	Uncertainty
Oven	a*	c	e	j		m	n
Hot Plate	a	c	e	j		m	n
Photonic	a*	d	e	j*			
Laser	a	d	f g	j			
Plasma	b	e	f h	l		m	n
Electrical	a*	d*	i	j*			NR
Microwave	a	d	o	i			p
Chemical	b	d	e	k			NR

Gray cells refer to the not reported fields. Refer to the reviews [7, 9, 10] and Table 5 for further detail on the listed information

a and *b* refer to the conductivity levels above and below 10^7 S/m (~ 6 times bulk silver resistivity) respectively. *a** near half conductivity of bulk silver was achieved. *c* 15 min to several hours, *c** several hours. *d* less than 5 min. *d** requires pre-heating *e* no related problems reported. *f* poor adhesion. *g* large pores. *h* non-uniform density. *i* abrupt roughness. *j* Thermal distortion at low thermal resistant substrates. *j** same type distortions also at high resistant substrates. *k* coatings and thermal process needed *l* no damage. “Cost” stands for technical and financial expenses, with green and red indicating low and high. *m* due to long processing times. *NR* not reported. *o* frequent hot spots, not up-scalable. *n* uncontrollable parameters. *p* placement dependent

these aspects, the most problematic issue comes as the damages given to the substrates by the employed curing methods, particularly to the ones with lower thermal resilience. The main reason for this is the fact that most curing processes (removal of the capping agents and diffusion of the conductive particles to form percolation paths) rely on exposing the printed films to heat. When the substrate exceeds its glass transition temperature, thermal distortions are likely to occur. While oven and hot curing methods expose the substrate+printed film to heat together, photonic curing, laser curing, electrical curing, and microwave curing methods aim to apply selective heating in order to reduce the thermal damage on the substrate [11, 12]. Microwave curing is the only of these methods, reporting non-destructive curing on a relatively low glass transition temperature substrate (PEN), at a short curing time and high conductivity. However, this method is yet not fully reliable due to the frequent hot spot occurrence [7].

The mentioned nonselective thermal methods are the most widely used methods due to their low financial and technical costs. However, they require long curing times (15 min to several hours), longer for the low thermal resistant substrates. Long processing times reduce the applicability of the methods for the cases such as rapid prototyping or R2R manufacturing, resulting in the loss of the advances the inkjet printing process introduces.

Selective thermal methods such as photonic curing, laser curing, and electrical curing on the other hand were reported to provide high conductivities in significantly short curing times, for high thermal

resistant materials. However, the rate and the mechanism of heating cause failures in the film quality, such as excessive pores, roughness, or poor adhesion to the substrate, which constitutes another critical limitation in the field. Furthermore, electrical and photonic curing methods were reported to thermally damage even the highly thermal resistant substrates [9, 12]. Photonic and laser curing also require much higher financial and technical investments compared to the other thermal curing methods [13], as well as the higher costs for thermal-resistant substrates.

To overcome the temperature-related issues, non-thermal curing mechanisms are also reported. Plasma curing being one of them, is one mechanism that was reported to perform safely on a low thermal resistant substrate. However, plasma curing comes with drawbacks in all other aspects, such as several hours of curing time, highly non-uniform film density, limited conductivity, and high cost [9]. Chemical curing method is a low-cost and rapid method to dissolve and remove the non-conductive compounds from the printed film, with chemical agents. However, some studies reported thermal sintering was still needed for sufficient conductivity [6, 7]. In addition, the chemical coating of the substrate prior to the printing limits the applications due to the coating technology such as double-sided printing [14].

Finally, the methods need to be robust and reproducible in order to avoid adding uncertainty to the final products. Flexible electronics especially applied in small-scale systems (such as soft robotics) are likely to introduce uncertainty and make the systems hard to estimate, model, and control. In such cases, fabrication

uncertainties become dominant, including the curing process effects [8, 15]. While the methods like laser and photonic curing potentially reduce the uncertainty due to their precise controllability, methods such as oven curing and microwave curing are less controllable and their contribution to the final device uncertainty is unknown [7, 9].

With this study, we aim to develop a new curing method, that enables fast, low-cost, efficient, and reliable activation of the inkjet printed Ag NP patterns, applicable for different substrates. We also aim to develop an understanding of the uncertainty introduced by the curing process, in order to eliminate or predict their effects on the final devices.

2 Methods

We propose and investigate a new curing method, using a laminator machine. We analyze the sample performances and uncertainties both for their electrical conductivity and for their application as angle sensors. In addition to experimenting with also oven curing (as being the most commonly used curing method) for direct comparison, we present a further evaluation of the proposed method compared with a wider range of curing methods in Sect. 4.2.1, based on the related literature. The flow of the used methodologies

is summarized in Table 2, details are given under the corresponding sections of the main text.

2.1 Inkjet printing

For the main set of experiments, a commercial Ag NP ink (NovaCentrix JS-B25p) is used [16]. The ink was reported to have an average particle size of 71.9 nm (95.5%–102.3 nm, 6.5%–14.53 nm) with 25wt% solid compound (Ag NP) [17–19]. It is defined as an aqueous dispersion by the manufacturer with polymeric capping agents surrounding the nano particles, that require curing to dissolve, and other volatile polymeric compounds of surfactant and humectant. The ink was reported to have polyethylene glycol 4 (tert-octylphenyl) ether as particle coating, and ethylene glycol as a solvent in [17, 18]. It has a 4.60 cP viscosity at 22°C, and the surface tension is 31.2 dynes/cm [17].

Usage of the ink with the pigment-based ink compatible office-type inkjet printers is well established and recommended by the ink company [4, 16, 17]. Samples are printed using an Epson L3150 office type desktop inkjet printer [20], following these criteria. Printer has a piezo printhead, with 180 nozzles for black and 59 nozzles per color (cyan, magenta, yellow). It has a 5760 × 1440 dpi print resolution, with 3 pl minimum droplet size.

Table 2 Summary of the methods and tools used to investigate and compare the effects of the developed lamination curing and the conventional oven curing

Process	Inspection	Tools
Printing	Pattern placement, Ink and substrate coating*	Inkjet Printer (Two types)*, Silver NP ink (Two types)*, Coated PET substrate, Uncoated PI substrate*, Pattern set I (Fig. 1c)
Oven curing	Sample size and placement, Curing temperature and times, Thermal distortion	Oven, Cut and whole samples (Fig. 1d, c),
Lamination curing	Curing temperature, Number of lamination cycles, Thickness of protective envelope layers, Feeding direction, Contact load by the rollers	Laminator, Thermo-resistor, Flexible force-sensitive resistance sensor
Electrical Conductivity tests	Sheet resistances, Dependency on the fabrication and curing parameters mentioned in the previous rows, Pattern geometry, Time-dependent shifts	van der Pauw method, LCR-meter, p-value correlation significance tests, Pattern set I & II (Fig. 1c, e)
Microstructural analysis	Particle aggregation, Surface asperities, Thickness	SEM
Angle sensing	Sensing parameters (see Fig. 11), Mechanical resilience	Angle sensor pattern (Fig. 1f), 3D printed bending setup, Bending tests
Curing efficiency analysis	Heat transfer effects	Lumped parameter model

Details are explained in the main text, under the corresponding sections

*The second type of ink, substrate, and printer are used only for the coating effect inspection

Ink is filled into all the printer cartridges. Printing parameters are set as; colored, highest quality, Epson premium glossy photo-paper. High speed print option is unchecked (note that later experiments with checked high speed option showed no significant difference in the sheet resistances and sensing behaviours of the printed samples).

As the substrate, the silica coated microporous PET substrate Novele IJ-220 by Novacentrix is used, as recommended by the company and well studied before [19, 21]. PET substrate has $140 \pm 12 \mu\text{m}$ thickness, and nanometer-scale pores at the surface which tunnel to depths of $20 \mu\text{m}$. The average surface roughness was reported as 10.7 nm . Surface architecture of the substrate facilitates the curing and the following sintering processes by letting the flow of the solvent into the substrate pores. It is also theorized the chemical agents in the coating diffuse into the nanoparticle film and helps the decomposition of the capping agents [8, 22]. A polyimide substrate ($125 \mu\text{m}$ thick Kapton) is also tested to inspect the curing performance on an uncoated surface. As the existing ink technology does not allow proper printing on the uncoated substrates by using desktop printers, we employed Dimatix Materials Printer DMP-2800, and the silver dispersion PN-736465 by Sigma-Aldrich. Ink has 30–35 wt% silver nanoparticle content (particle size $\leq 50 \text{ nm}$) in triethylene glycol monomethyl ether. Its surface tension is approximated as 35–40 dyn/cm and viscosity as 10–18 cp [23]. A single nozzle of the print head with a 10 pl drop size is used. Drop spacing was set to $20 \mu\text{m}$, and

the printed drop diameter was measured as $60 \mu\text{m}$. The platen temperature was 50°C .

Two sets of patterns are used for the experiments. Pattern set I (Fig. 1c) consists of 9 equally distributed $1 \times 1 \text{ cm}$ squares (3 columns and 3 rows) to inspect the placement (or printing order) effects on the sheet resistances and the reproducibility. To define the uncertainty, the mean relative standard deviation value is calculated as,

$$\text{mean relative SD} = \frac{\sum_i^N \frac{\sigma_{c,i}^2}{\bar{c}_i}}{N} \quad (1)$$

where N is the number of columns and σ_c and \bar{c} are the standard deviation and mean of the sheet resistance values within a column.

2.2 Curing

2.2.1 Oven curing

Memmert UN 55 natural convection laboratory oven [24] is employed for the oven curing experiments. 100°C and 120°C curing temperatures are tested for 15, 25 and 60 min curing times to investigate the curing capabilities. (Note that above 120°C , the PET substrate starts to distort profoundly due to its low glass transition temperature of 70°C .) Placement of the samples into the oven and the oven timer setting are done only after the oven reached the set curing temperature.

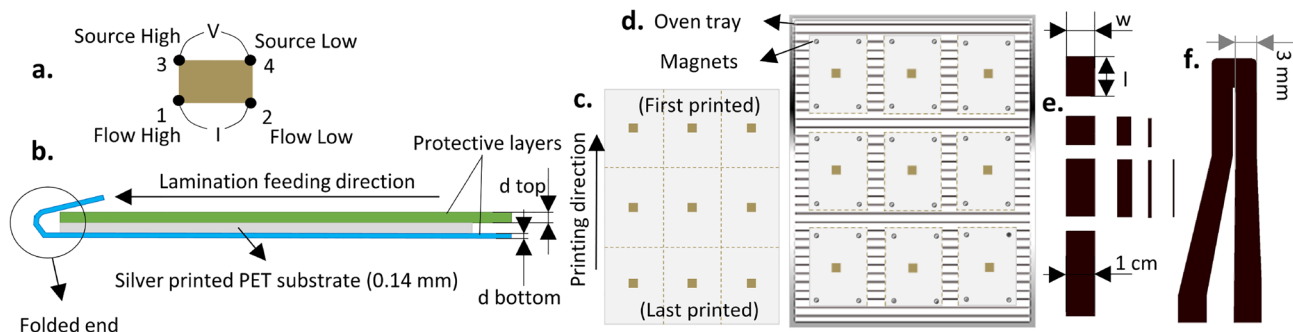


Fig. 1 **a** Measurement configuration used with the four terminal LCR-meter for a sample with an arbitrary aspect ratio. A square sample is used for the van der Pauw method measurement (c–e). **b** Schematic representation of the lamination configuration of the silver patterns printed substrate and sandwiching protective layers. The edge of the thinner layer is folded at the feeding side, to avoid any slip between the layers. **c** Schematic representation of a

printed sample (pattern set I) at uncut configuration. **d** Schematic representation of sample placement on the oven tray for curing at cut configuration. PET substrate is fixed on the tray with magnets at the corners. **e** Pattern set II, used for the pattern geometry and time-dependent shift experiments. **f** Angle sensor patterns used in the bending tests

Oven air flap is set 50% open for all experiments due to the expected evaporation of the solvents.

Placement into the oven (positioning of the tray) and the size of the samples (cut or whole) are also considered as the parameters in the uncertainty analysis, as they were observed to affect the resulting resistances during our previous studies. Among the 4 levels of slides in the oven chamber, level 2 and 3 (numerated from bottom to top) are tested with cut (Fig. 1d) and uncut letter-sized (whole) samples (Fig. 1c). Oven cured sample data all together had a population number of 171. *p* value correlation significance test is used to detect the possible dependencies of the sheet resistances to the mentioned parameters.

2.2.2 Lamination curing

A low-cost (<150\$) desktop laminator, Olympia A 3048 [25], is used to cure the printed samples. The device uses two pairs of heating roller presses to laminate foils in a range of 80 to 250 μm of thickness. While the method does not involve the lamination of any extra layers on the samples, it benefits from the heat and the pressure the rollers apply on the printed film.

Heating levels of the laminator device are originally defined in μm based on the targetted foil thicknesses. Corresponding temperature levels are estimated to be in the range of 130 to 170 $^{\circ}\text{C}$, by passing a thermistor through the laminator. The contact load applied on the substrate for a total thickness of 500 μm is estimated as 5N/cm, by passing a 1 cm width force-sensitive resistor (RP-L-170 [26]) through the rollers.

PET layer is enveloped between two paper layers to avoid direct contact with the rollers (Fig. 1b). Three heating levels of the device (80 μm (130 $^{\circ}\text{C}$), 125 μm (140 $^{\circ}\text{C}$), 250 μm (170 $^{\circ}\text{C}$)) are used with different protective paper thicknesses and numbers of lamination cycles (number of pass) to optimize the curing process. Device has a 600 mm/min laminating speed and a warm up time about 3–5 min at room temperature.

For the investigation of the effects of the pattern placement, printing direction (order), and feeding direction into the laminator, uncut samples (pattern set I, Fig. 1c) are fed into the lamination machine in both the opposite direction (feed direction 1) and the same direction (feed direction 2) as the printing direction (Fig. 1b). Lamination cured samples are analyzed in two populations, population 1 ($n = 36$) fed in direction 1, and population 2 ($n = 45$) fed in direction 2. 24

members of population 2 were cured after being cut into single columns and not included in the column dependency analysis. *p* value correlation significance test is used to detect the possible dependencies of the sheet resistances to the mentioned parameters.

2.3 Electrical conductivity inspections

Sample resistances are measured with the LCR-meter with the configuration in Fig. 1a, by directly contacting the device probes on the corners of the printed patterns. In order to obtain the sheet resistances (i.e. surface resistivity, square resistance), van der Pauw technique is preferred as it is a more feasible method for small sized patterns compared to the four probe method [27, 28]. The square pattern resistances ($R(r_a)$ at aspect ratio $r_a = 1$, Fig. 1c–e) and (2) are employed.

$$R_{sheet} = 4.532 \cdot \frac{V_{34}}{I_{12}} \quad (2)$$

I_{12} is the current flow given to the specimen through points 1 and 2, and V_{34} is the measured voltage drop between points 3 and 4, are employed [27]. To estimate the conductivity from the surface resistivity, cured film thicknesses are measured approximately using the cross section images captured with SEM. In order to investigate the pattern geometry effect on the sample resistance, and the shifts in the sheet resistances with the time, the pattern set II (Fig. 1e) consisting of 9 rectangles with varying aspect ratios (1 to 50) is printed and cured with both curing methods. Lamination curing configuration is selected as described in Sect. 2.4. Oven curing is performed at 120 $^{\circ}\text{C}$ (higher temperature) and 15 min, to compare with the most stable resistances.

2.4 Microstructural inspection

The microstructures of the printed samples cured with the proposed lamination method and the conventional oven curing method are inspected under SEM to compare the curing effects. Curing parameters are selected as the ones that are found to provide the best performance (lowest uncertainty, lowest resistance, least thermal distortion) for both methods: Oven curing at 100 $^{\circ}\text{C}$ for 60 min, Lamination curing at 170 $^{\circ}\text{C}$, with 3 passes, and 0.12 and 0.21 mm top and bottom protective paper layers (Sect. 3). Following the printing and curing of the samples, they are bent to form a crack

and inspect the film over this cross-section, as well as the surface.

2.5 Sensor behaviour testing

As a case study, resistive angle sensors (Fig. 1f) are printed, and cured with both methods, to test the possible curing method effects on the electromechanical properties and the mechanical behavior of the film and the PET substrate.

A 3D printed setup is used to test the angle sensor behaviors of the samples (Fig. 2). Sensors are bent from 0° (flat position) to 90° both in compression and tension directions. The approximate radius of curvature of the sensors at 90° is 1 mm. Sensor responses are measured with a simple voltage divider circuit and a 14-bit data acquisition card at 20 Hz. The rotational joint is actuated with a servo motor (Dynamixel XL430-W250-T).

A triangular wave between 0 – 90° at 10 sec period and a stepwise trajectory of 10° steps with 5 s stops from 0 to 90 and back to 0° are used for the tests

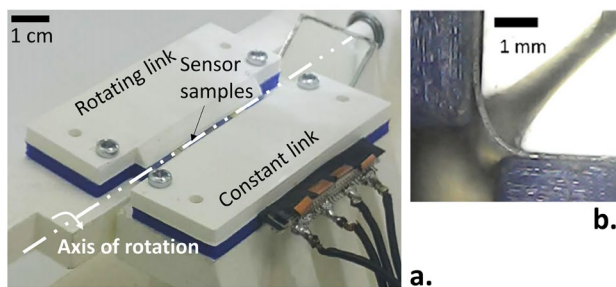


Fig. 2 a Experimental setup used for testing the cured samples under low radius of curvature bending for an angle sensing application case. b Side view of the samples at 90° bending angle

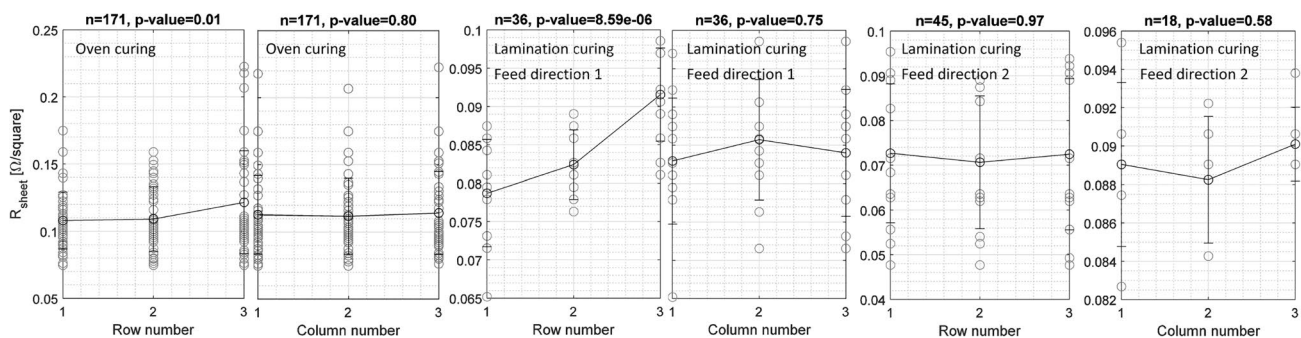


Fig. 3 Sheet resistance distributions w/to column and row numbers of the square patterns in pattern set I. Lamination curing in feed direction 2 shows the lowest dependency on the row number. n stands for the popular, on numbers of the experiment groups

(graphically represented in Sect. 3.6). Stepwise trajectory is applied with two different deceleration profiles (sharp and smooth) [14] to investigate the robustness of the sensor behaviours to dynamic effects. Mean resistance data is obtained from last 1 s of each step. Cyclic and static drift, % resistance change, nonlinearity, hysteresis, and dynamic dependency characteristics are considered. They are calculated and tested as in [14]. An overall score is calculated with the formulation in (3) based on all performance parameters (p) (listed in Fig. 11).

$$\text{Overall Score} = \frac{\sum_i n_p \frac{p_i - p_{\text{worst}}}{p_{\text{best}} - p_{\text{worst}}}}{n_p} \quad (3)$$

Experiments are done with 4 separate sensor samples for the oven and lamination curing methods. Lamination and oven curing parameters are set as described in Sect. 2.3. Two samples are tested on the fabrication day and two on the day after.

3 Results

3.1 Fabrication uncertainty

Figure 3 shows the row and column dependency of the sheet resistances for oven and lamination curing. Oven cured sample data showed a statistically significant correlation (p value < 0.05) with the row number (i.e. printing order). Results indicate that the first printed patterns tend to have lower sheet resistances than the latter. No dependency is observed on the column number.

Although lamination in direction 1 had an even higher dependency to the row number than the oven cured samples, no significant correlation existed when the feeding direction 2 is applied in lamination curing. No correlations are found with the column number.

Table 3 presents the results for the resistance deviation inspection within a column. Row deviation is neglected based on the results presented above. A combined configuration for the oven curing (cut & level 2) showed the lowest deviation (2%). Lamination curing in feed direction 2 yielded a 3% uncertainty. Overall resistance variations within the columns were 37% lower with lamination curing.

Table 3 Uncertainties of oven and lamination curing methods, in terms of mean relative standard deviation within a column of printed samples

Oven				Lamination	
Whole (N = 24)	Cut (N = 21)	Level 2 (N= 21)	Level 3 (N = 24)	Feed dir. 1 (N = 12)	Feed dir. 2 (N = 15)
11%	5%	5%	12%	9 %	3%
Cut + Level 2: 2 % (N = 9)				Overall: 5 % (N = 27)	
Overall: 8 % (N = 57)					

N is the number of sample columns

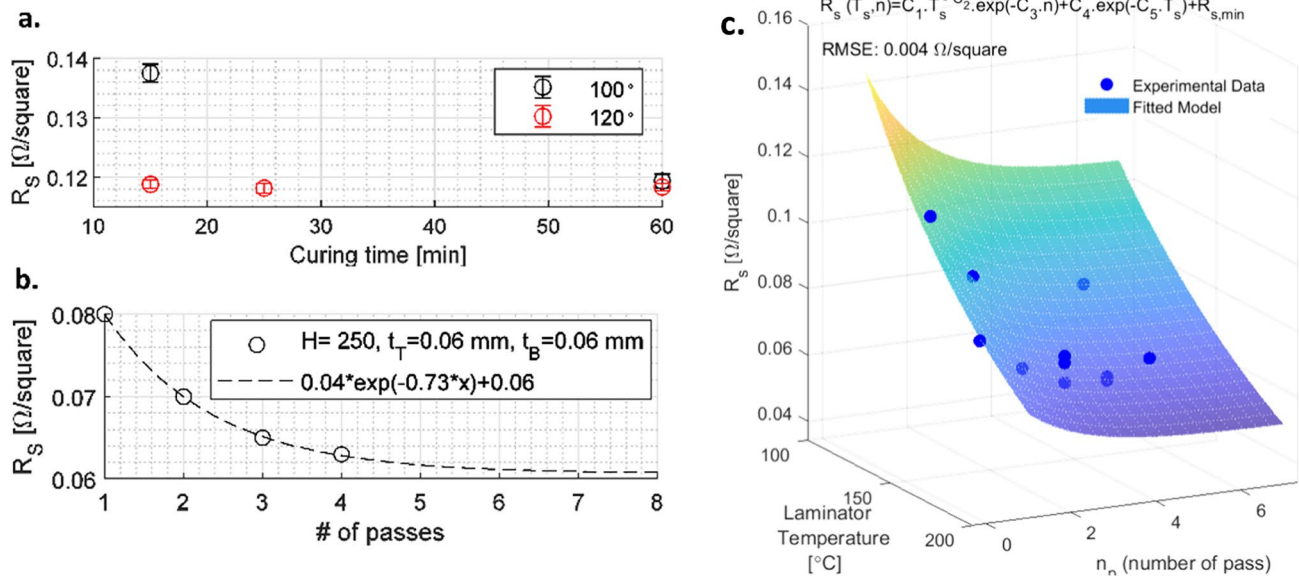


Fig. 4 a Sheet resistance dependency on the oven curing temperature and curing time. b Sheet resistance dependency on the lamination pass number is represented with an exponential func-

3.2 Curing parameters

3.2.1 Oven

The minimum attainable sheet resistance for the printed samples are found to be 0.12 Ω/□ with the oven curing (Fig. 4a). While 15 min of curing at 120 °C was sufficient for achieving this value, a safer temperature for the PET material, 100 °C, needed an hour of curing time.

Due to the low glass transition temperature of PET (~70 °C) visually inspected samples showed noticeable shape distortions (folding) after the thermal process, despite the magnets placed to fix the samples

tion. c Sheet resistance model as a function of laminator temperature (T_s , s: source) and number of pass (n_p)

onto the oven grid (Fig. 1d). While the distortion was observed at both temperatures and for both the cut and uncut PET sheets, shape changes were more dominant in the cut samples and at 120 °C.

3.2.2 Lamination

Used curing parameters and the resulting sheet resistances are listed in Table 4. While the protective cover papers used did not affect the resulting sheet resistance, at certain thicknesses they showed form distortions due to the heat and pressure applied, causing undesirable traces on the printed samples. At 120 and 210 μm top and bottom paper thicknesses, curing was performed without any paper crease and visible trace on the substrate. We note that the curing tests done without any protective papers did not cause any deformation on the film or the substrates, and gave the same resistance values. However, protective layer usage is recommended to avoid any contamination between the rollers and the conductive films and avoid damage in case of a potential paper stuck. Lamination cured substrates did not show significant shape change due to any thermal distortion, despite the much higher temperatures applied to the samples compared to the oven curing. Resting the sheet between flat surfaces following the lamination passes, completely eliminated the subtle bending of the PET sheet.

Experiment results showed that the sheet resistance of the samples tends to decrease exponentially with number of passes at constant curing temperature (Fig. 4b). 3 lamination passes at 250 μm heat level (170 °C) provided sufficient curing and provided sheet resistances down to 0.064 Ω/\square . Further cycle contributions were insignificant. Using the experimental data

presented in Table 4, an experimental model is built to predict the lamination parameter effects on the resulting sheet resistance.

$$R_s(T_s, n) = C_1 \cdot \frac{e^{-C_3 n}}{T_s^{C_2}} + R_{s,min} + C_4 \cdot e^{-C_5 T_s} \quad (4)$$

The first term of the equation represents the exponential decrease in the resistance with the number of passes. Laminator temperature term in the denominator adjusts the gain of the exponential, indicating decreasing effect of lamination passes at lower temperatures. The second and third terms of the equation define the lowest sheet resistance value the sample will converge at a certain temperature. The exponential term at this part indicates that this bottom value will decrease exponentially with the increasing curing temperature, and converge to a min value, $R_{s,min}$, corresponding to the maximum attainable conductivity in theory. $R_{s,min}$ for the model represented in Fig. 4.c is 0.014 Ω/\square corresponding to the 80% conductivity of bulk silver. The model gave a 0.004 Ω/\square RMS goodness of fit. Other parameters in the model from C_1 to C_5 are 77.97, 1.5, 0.73, 0.2206, and 0.008754, respectively.

3.3 Pattern geometry and time effects

Sheet resistances for the oven and lamination cured samples are found 0.09 Ω/\square and 0.14 Ω/\square at the fabrication day. 18th day data showed 6% and 8% decline, respectively. Difference between the shift ratios of the two curing methods was insignificant based on the measurement uncertainty which was calculated as 2%.

Obtained sheet resistances differed from the ones obtained from pattern set I previously (on another fabrication day), for both curing methods. To investigate this, in Fig. 5b ($R_{S,Oven}$, $R_{S,Lamination}$) data pairs belonging to different samples fabricated at different days

Table 4 Sheet resistances with varying lamination parameters. T and B stands for top and bottom paper layer thickness in μm

Heat level	T	B	Number of passes & R_s [Ω/\square]					C
			1	2	3	4	5	
80	60	20	–	–	–	–	0.08	Y
125	60	60	0.11	0.09	–	–	–	Y
250	60	60	0.08	0.07	0.07	0.063	–	Y
	120	120	–	–	–	0.064	–	Y
	60	210	–	–	0.064	0.064	–	Y
	120	210	–	–	0.072	–	0.068	N

C stands for paper crease and Y & N for yes & no

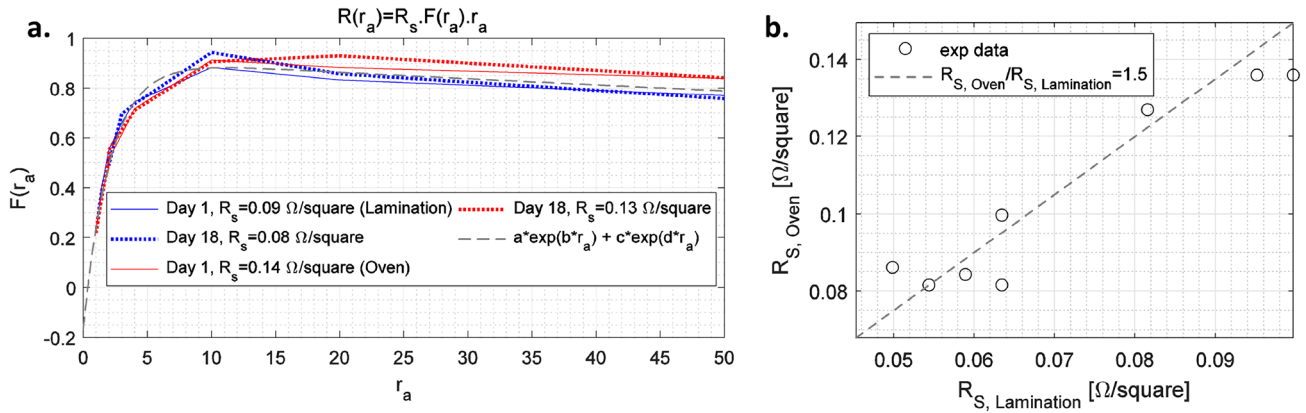


Fig. 5 a Experimental model for the sheet resistance geometric factor $F(r_a)$. R_s is the sheet resistance obtained with the Van der Pauw method, r_a is the aspect ratio of the printed pattern and F

is a geometrical factor. $a = 0.918$, $b = -0.003$, $c = -1.083$, $d = -0.473$. **b** ($R_{S,Oven}, R_{S,Lamination}$) data pairs belonging to different days of fabrication

are plotted. A constant ratio between the two curing methods is detected.

In order to compare specimen resistances at different aspect ratios cured with two methods, measured resistances (R_{r_a}) are expressed in terms of sheet resistance as in 5, where F is defined as a coefficient dependent on r_a .

$$R_{r_a} = R_{sheet} \cdot r_a \cdot F(r_a) \tag{5}$$

Figure 5a shows the F curves obtained with two curing methods do intersect. Notice $F(1)$ on the graph corresponds to 0.22 (1/4.532) based on (5). However, F does not converge to 1 with the increasing aspect ratio, which yields a discrepancy between the sheet resistance values obtained with van der Pauw method and values that number of squares method would give. $F(r_a)$ is approximated with the exponential function given in Fig. 5a.

3.4 Microstructure

Microstructure images are given in Fig. 6. The average thickness of the oven and lamination-cured samples are measured as $1.6 \mu\text{m}$ and $1.3 \mu\text{m}$, respectively, pointing to an increased density and the electron concentration of the latter [29]. The lamination cured sample also showed better aggregation of the particles, indicating a higher percolation (better diffusion), and a more uniform distribution of the thickness and the surface topology. Lamination cured sample showed

larger and flattened asperities on the surface. The regions by the surfaces (shells) showed higher particle growth for both samples. In the lamination cured sample, shells are observed thicker.

3.5 Applicability on uncoated substrate

Figure 7 shows lamination curing method (as well as the oven curing) was successful at decreasing the sheet resistances of the samples down to $0.05 \Omega/\square$, despite the absence of any additional facilitating agent by a chemical coating on the substrate.

3.6 Angle sensor behavior

Samples cured with two methods are found to show similar sensor characteristics (Figs. 8, 9). Mean sensor resistances are measured as 1.6 and $2.1 \Omega/\square$ respectively. Lamination cured sensors gave a higher resistance change ratio (higher gain). They also tended to show lower static and cyclic drifts. SNR of the lamination cured samples are observed higher and less varied. Although lamination cured samples showed higher nonlinearity, deviations in the RMSE were lower (Fig. 11). Lamination cured sensors showed similar behaviours for both smooth and sharp trajectory profiles where oven cured sensor responses differed (Fig. 11). Lamination cured sensors gave better overall performance (by 3) than oven cured sensors with higher consistency (Fig. 10).

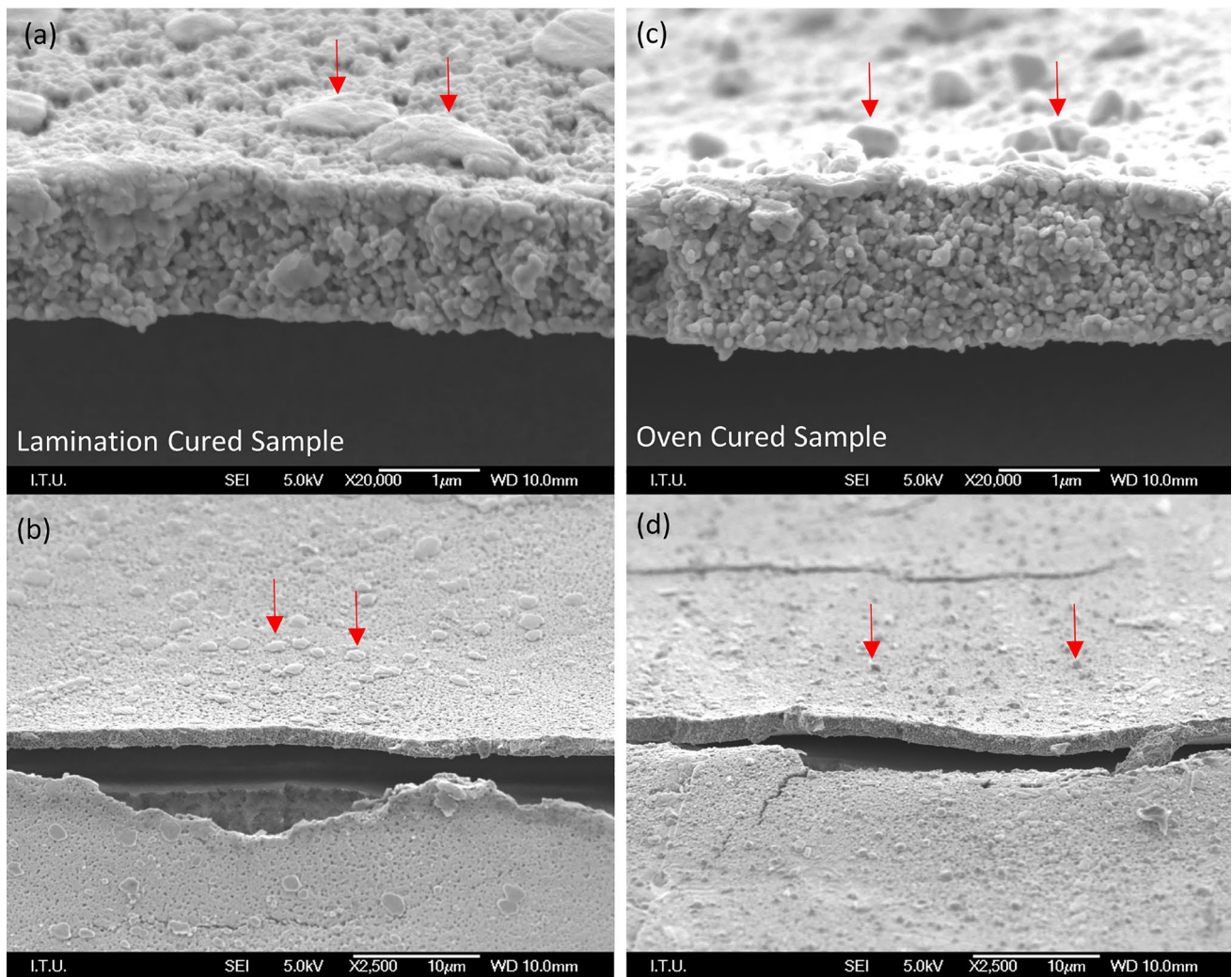


Fig. 6 SEM images of the lamination and oven-cured samples of the Ag NP inkjet printed sensors on PET substrate. Red arrows show the asperities on the printed film surface, flattened on the

lamination cured sample. 100 °C and 170 °C temperatures are used for the oven and lamination curing respectively

4 Discussions

4.1 Effects of the lamination curing

The experiments showed that, with lamination curing, similar or higher conductivity levels than the ones obtained with oven curing are achieved, at similar or higher curing temperatures, in dramatically shorter curing times, and without damaging the substrates despite the temperatures (~170 °C) highly over the PET glass transition temperature (70 °C), and the damages observed with oven curing at lower temperatures (100–120 °C).

Regarding the experiments performed with PI, which enabled higher oven curing temperatures compare to PET, thus similar curing temperature with the lamination curing (150 ° vs 170 °), we see that lamination curing at this condition did not provide any further increase in the achieved conductivity, but provided a much shorter curing time resulting with the same conductivity. Whereas the 3 passes of the lamination correspond to 3 min due to the A4-sized samples, the actual curing speed can be approximated by the estimation of the contact area, and the feeding speed of the lamination machine [30]. Referring to the contact model given in [31] and the measured contact load, we estimate the contact width as 1.4

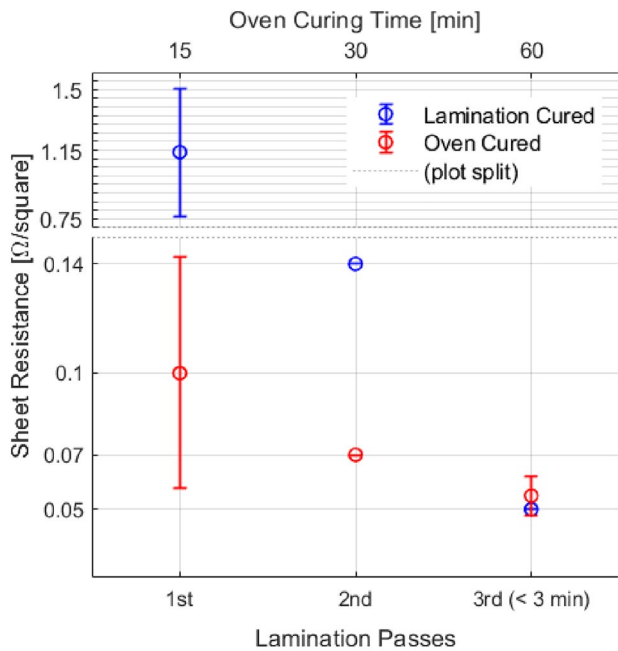


Fig. 7 Lamination and oven curing performances for the Ag NP prints with Dimatix inkjet printer on an uncoated polyimide substrate. 2 printed samples are used to test each curing method

mm. Assuming a uniform temperature distribution on the contact width for simplicity, we can conclude that a point on the lamination-cured sample spends only 0.42 s between the laminator heated roll presses, based on the 3.3 mm/s constant feeding speed. Regarding that the samples were passed 3 times through the machine, and neglecting the potential temperature drops in between the successive passes, a 1.3 s can be assumed. This corresponds to a $\times 692$ decrease in the curing time as a thermal process compared to oven curing, which is dramatic, especially considering the similar temperatures applied.

Regarding the potential reasons behind the increased curing efficiency, we first consider the fact that the curing temperature was 20 °C higher with the lamination curing. However, both based on the curing parameter models we built in this study, and both on the related literature, it is not likely to achieve this level of curing time, with oven curing. Escobedo et al. [12] presents a detailed study on this and the lowest attainable curing time with oven was 1.5 min and at 200 °C. This was only the rise time, and the settling to the minimum resistance value for the corresponding temperature took 60 min. Thus we conclude that a mechanism other than the higher curing temperature is likely to cause this efficiency.

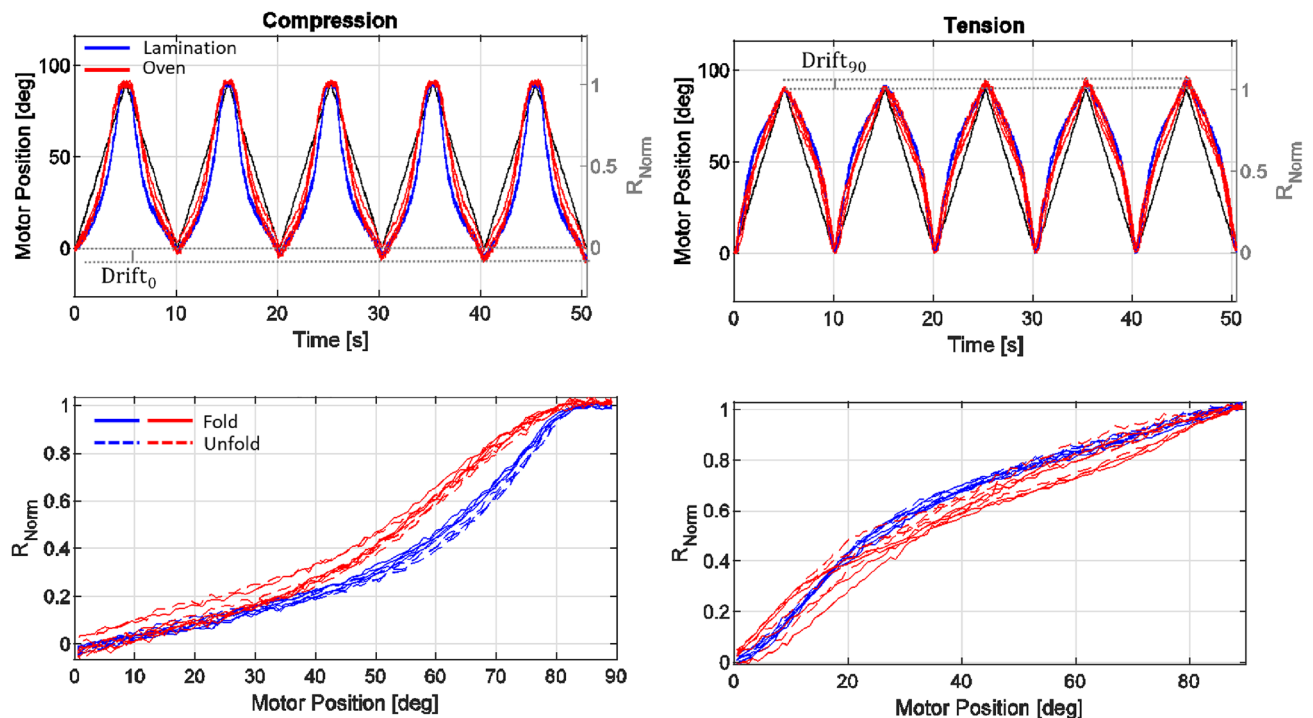


Fig. 8 Triangular wave responses of four oven cured and four lamination cured angle sensor samples

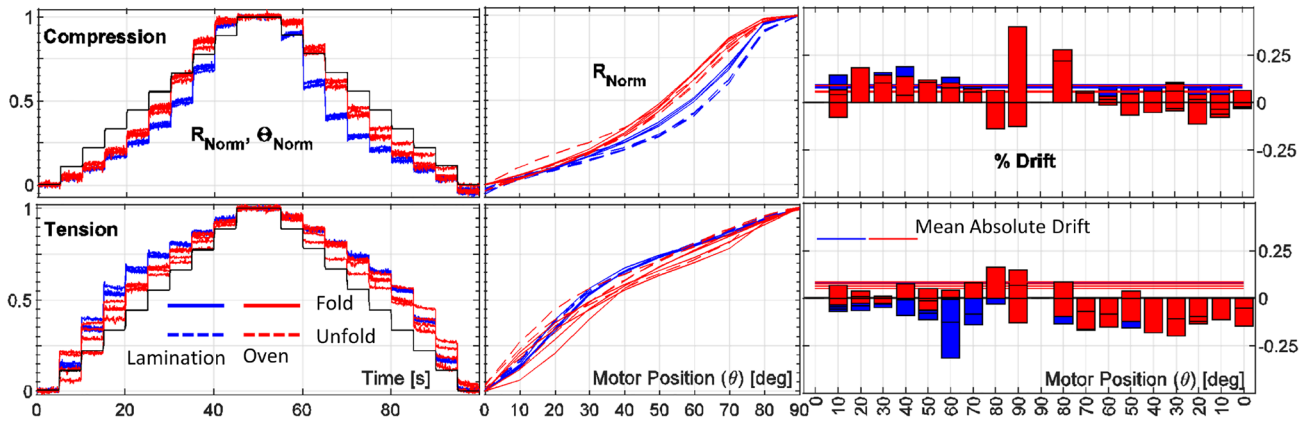


Fig. 9 Step responses of four oven cured and four lamination cured angle sensor samples. Higher deviation is observed in the oven cured samples both in time response (column 1), mean steady state response (column 2) and static drifts (column 3)

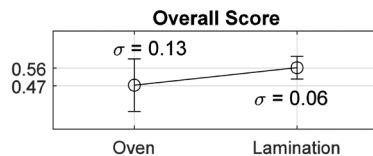


Fig. 10 Overall score of the sensors ($N = 4$). Lamination cured sensors gave a higher performance with lower uncertainty

Pressure on the other hand is known to be a parameter, such like the temperature, enhancing the sintering process, by increasing the density, and the diffusion between the particles [10]. While it did not

increase the final conductivity attained, it might have accelerated the particle diffusion by several mechanisms. Due to the office laminator we used not being pressure adjustable, the potential independent and combined effects (with the temperature) of the lamination pressure are not known by our study.

Another significant advance the laminator brought was the over-glass transition temperature curing without any visible damage on the substrate. In contrast, the oven-cured samples caused distortion of the PET, at 100 and 120 °C. To understand the underlying mechanism, we discuss the possibility of a selective type of heating occurring on the silver-printed

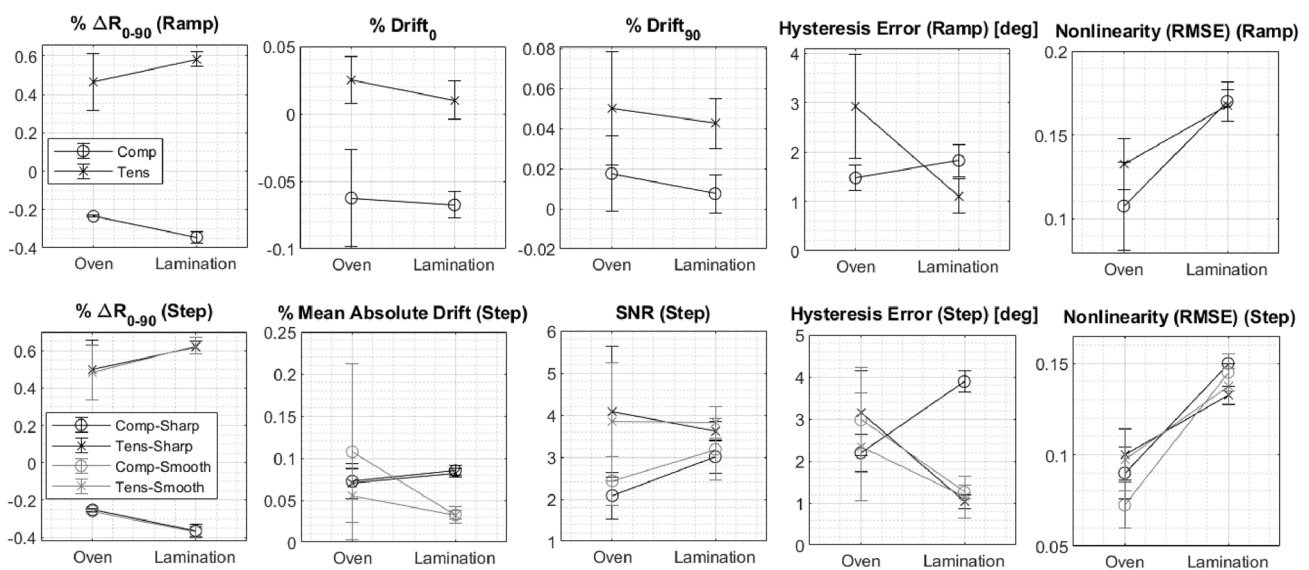


Fig. 11 Performance statistics of four oven cured and four lamination cured angle sensor samples. Lamination curing gave higher performance at all metrics except nonlinearity, and lower uncertainty at all metrics

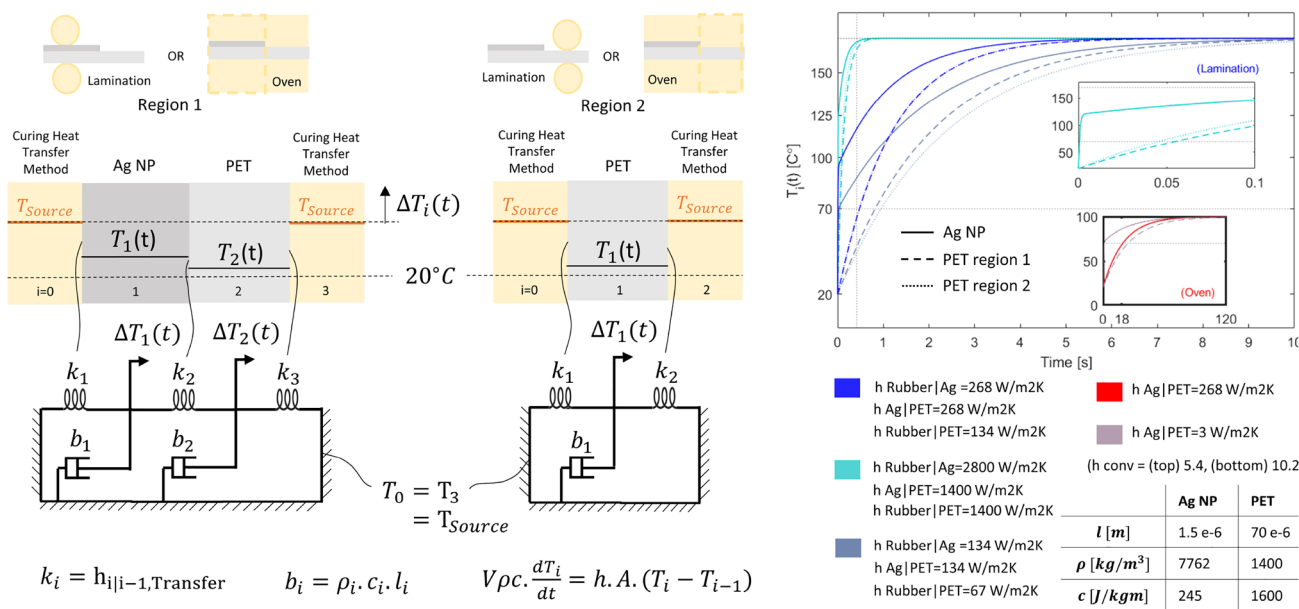


Fig. 12 Lumped parameter model for the transient temperature responses during the curing processes. For the density and heat capacity of the silver film [35] is referred

substrate, based on the thermal property differences of the Ag NP print and the PET substrate, and only 0.42 sec per pass heat exposure time. In other words, we investigate the possibility of the sample passing through the laminator rolls, at a rate at which the PET substrate yet not reaches the glass transition temperature (i.e. 70 °), yet, the silver film reaches the targeted curing temperature (i.e. 170 °).

In order to inspect this theory, we perform a transient analysis on the heat transfer rate from the laminator rolls to the substrate and the silver film. Figure 12 shows the built model. The heat flow is caused by the potential (i.e. temperature) difference between the heat source (laminator rolls) and the sample. The rate of the heat flow is determined by the conductance through its way, of the materials (roller, silver, PET) and their interfaces (thermal contact conductance [32–34]).

Hussain et al. [35] models and calculates the transient temperature distribution on a Ag NP film printed on a thick glass substrate, during laser sintering. They use FEM modelling and find out that silver film was thermally thin (its temperature distribution along its thickness was constant) unlike the glass substrate. They neglect the thermal contact resistance between the silver film and the glass substrate. Lu and Pagilla

[30] models the heat transfer from the rollers to the web, both by assuming and neglecting the thermal contact resistances, and assuming a non-uniform distribution of the temperature through the material thickness.

We built a lumped parameter model, assuming constant temperature distribution through the materials thicknesses thus neglecting the internal thermal conduction resistances of the materials compared to the interface resistances. This approach is explained in [36] in detail over the convection conductance (air - solid interface), and require the interface conductance to be less than 0.1x of the material bulk conductance [33]. Recalling our experiment results which showed the protective layer existence and thicknesses did not affect the resulting performance, we used the direct contact case to model for simplicity. For our case the thermal contact conductance values taken from the literature at the same temperature and pressure values for polymer-polymer [34] (for rubber roller-PET contact), and metal-polymer [33] (for rubber-Ag NP and Ag NP contacts) contact interface are found dominant due to the low thickness of the silver and PET films (based on [36], see the light-blue legend set for the numerical values). This allows us to build the lumped

parameter model, counting for the interface resistances only.

Referring to the operating temperatures, we assume no phase change [35]. We formulate the heat transfer problem as an initial value problem using the state space model. The source temperatures (roller surfaces) are taken constant. (Parametric and numerical values of the state space model matrices derived from the spring-damper analogy model in Fig. 12 are provided in the supplementary material, as well as the code syntax for the solution.)

The resulting heat transfer equation defines the transient time response of the system, based on the time constants defined by:

$$\tau = \frac{\rho \cdot l \cdot C}{h} \quad (6)$$

However, due to the layered structure involved, the system we analyze here is multi-modal and the temperature responses of the silver and PET film are coupled. In order to test our hypothesis of selective heating, we simulate the model numerically for both the case rollers touch to the printed area (region 1 in Fig. 12) and empty PET (region 2). The dark-blue curves in Fig. 12 shows that based on the values taken from the literature and the model we built, after rollers at 170 °C are touched to the printed samples initially at room temperature, the PET temperature remains slightly below the glass transition temperature, when its contact ends with the rollers (PET at region 1 and 2 gave similar results). This result we found is consistent with the experimental observation of the PET not being damaged after passing the lamination rollers.

As a next step we inspect the silver film response. The model clearly shows that the silver temperature rises with a dramatically higher speed. This is due to the dominance of the fast converging exponential component of the coupled response (the lower time constant). The significantly lower thickness and heat capacity of the silver, allowed by the high enough thermal contact conductance (Table in Fig. 12) causes the fast component of the response. However, after this rapid increase, the temperature rise is slowed by the dominance of the higher heat capacity of the PET material, thus the silver material remains at 125 °C when it exists from the laminator. This indicates that according to this model, and the referenced values from the literature, curing occurs at a lower temperature than the assumed (measured roller surface temperature). The temperature of the roller was measured

by a small sized 3D hard component thermistor, which potentially increased the pressure and provided a closer temperature measurement to the actual temperature of the roller. All in all, 125 °C is still a sufficient temperature for the curing, and supports the idea of pressure catalyzed sintering.

On the other hand, thermal contact conductances are parameters delicate to measure and estimate, and dependent on several factors [32]. The real contact area is one of the most important factors defining it. With the light-blue curve in Fig. 12, we assume a much higher contact conductance, due to the 3 orders of level lower elastic modulus of the rubber (laminator roller), than the referenced polymer in [33]. In order to simulate an extreme case, we increased the contact conductance to an order of magnitude higher value. We limited the conductance at PET interfaces to the thermal conduction conductance of the PET material, as at this extreme condition the lump parameter criteria (the dominance of the interface conductance) does not apply anymore. This case showed that the silver layer could reach the roll temperature in time, however, the PET layer passed the glass temperature at only 0.05 s. For this case scenario, the temperature analysis through the PET thickness and the dynamics of the thermal distortions over glass transition temperature can be further investigated to evaluate the sufficiency. This scenario also gives an insight to the parameters effects and optimization scenarios for the future studies. With an increased pressure, lower roller radii and faster lamination feed can be tested to compensate the reduced glass transition time.

Finally with the gray curves we demonstrated a lower conductance case, due to the granular and porous surfaces of the silver and PET layer, which may decrease the effective contact area. This case resulted with Ag staying at 90 °C and PET temperature ending up in a much safer region below glass transition. While the silver temperature is relatively low, [4] showed that it is still a sufficient temperature for curing the Ag NP on PET (with oven, in 60 min), but with a much lower resulting electrical conductivity than our study (Table 5).

We analyzed the oven curing process as well, using the same model. Computation of the natural convection conductance for this case is straightforward (provided in the supplementary material). Natural convection conductance has an even lower magnitude, thus complies with the lumped parameters assumption (Fig. 12). Red curve shows the case where we assumed

Table 5 Curing method performances comparison for inkjet printed Ag NP films

Curing method	Printer	Substrate	Conductivity (.10 ⁶ S/m)	Print thick- ness (μm)	Sheet resist- ance (Ω/□)	Time (min)	Other	
Conventional methods								
Oven	Office	PET	2	1.9	0.25	60	90 °C	[4]
Hot plate	Dimatix	PET	12	1.25	0.07	30	120 °C	[39]
Oven	Dimatix	PI	27	0.8	–	60	220 °C	[9]
Oven	Office	PET	7	–	–	–	100 °C	[16]
Oven	Office	PET	7	1.6	0.09	15	120 °C	This study
Oven	Dimatix	PI	–	–	0.05	15	150 °C	This study
Proposed method								
Lamination	Office	PET	12	1.3	0.06	<3 (3.3 mm/s)	170 °C	This study
Lamination	Dimatix	PI	–	–	0.05	<3 (3.3 mm/s)	170 °C	This study
Alternative methods								
Photonic	Office	PET	–	–	0.06	–	–	[16]
Photonic	Dimatix	PI	30	1.5	0.02	10–40 s	–	[9]
Laser	Dimatix	PI	22	5	0.01	100 mm/s	–	[9]
Plasma	Dimatix	PC	7	0.6	0.23	240	–	[9]
Microwave	Autodrop	PEN	6–21	–	–	1–60 s	–	[11]
Oven + Electrical	Dimatix	PI	33	0.8	–	4+0.2	100 °C + (–)	[12]
Chemical	Office	PET	–	–	0.2	Instant	Self-curing ink	[5, 40]
Chemical + Oven	Office	PET	–	1.5	0.1	30	Self-curing ink, 60–150 °C	[6]

Proposed method has the advantage of low curing time and high conductivity on PET substrate. Note that the lamination method also holds the advantage of allowing higher temperature curing without thermal distortion of the substrate

the contact conductance between the silver and PET same as the lamination case. Here, the low efficiency of the convection relative to the PET-silver interface avoided the material properties (ρ, c, l) to dominate the response, and selective heating is not observed. Due to the lack of contact pressure, the conductance at PET-silver interface is expected to be much lower [34]. Purple curve in Fig. 12 showed that reducing this conductance at a value below convection conductance retained the selective heating, however the glass transition temperature is reached at 18 sec, which is not allowing a sufficient oven curing time.

As a result, the most common orders of values in the literature for the targeted type of interfaces at the experimented pressure levels showed that the selective heating of the PET and silver layer is allowed by the both curing methods, based on our model. However, only lamination curing (with the potential effect of pressure) provides the sintering of the silver nanoparticles in such a short time, before the glass transition is passed. Recalling the challenges in the prediction of contact resistances, and replication of the curing performances with the protective layers included, further

experiments on the dominant thermal resistances and the pressure effect would be beneficial to conclude on the working principle.

4.1.1 Uncertainty, durability and angle sensing

Our analysis showed that a reduced uncertainty for the oven curing method came only with the cut samples placed at a single tray, thus with the cost of limiting the max size and number of samples at a single curing batch. This indicates a limitation for the total time needed for the curing process, for multiple samples. Memmert Operating Instructions [37] points out that the loading of the large and irregularly placed samples (A4 sized relatively large are samples for our case, compared to the cut and distantly placed samples) into the oven avoids proper circulation of the air, and may result with inaccurate and non-homogenous temperature distribution on the samples. On the other hand with lamination curing the uncertainty was significantly reduced. A well-functioning lamination roller is expected to apply a homogenous pressure

and temperature along its rolling axis [30, 38]. Thus, we suggest the reduced uncertainty (half the oven cured sample uncertainty) along the row patterns indicate that lamination machine provided homogeneous boundary conditions for the curing, independent from the sample size. Oven cured sample resistances showed a significant dependency on the printing order, where lamination curing completely eliminated this dependency in one direction and increased at the opposite direction of lamination feed. While this indicates a potential bias of the samples dependent to the printing order, underlying reasons under this observation needs further inspections. Lamination cured angle sensors are found to perform better in all metrics, except nonlinearity. However, both the nonlinearity and overall score of the lamination cured sensors showed half the deviation observed in the oven cured sensors. This indicates a higher calibration accuracy for the sensors and a reduction of the uncertainty effects on the final devices, together with the lower fabrication uncertainty recorded. With the lamination parameters used in this study, no failures in the film or the substrate are detected after 5000 cycles of bending [14]. On the other hand, the distortions occurred on oven cured samples formed fractures on some sample substrates when bent during the sensor tests, and caused some of the sensors to lose their conductivity. These sensors had to be replaced with new ones to complete the experiments.

4.2 Consistency and comparison with the related literature

4.2.1 Curing methods

Table 5 summarizes the electrical conductivity characteristics reported in the literature, for oven curing and other known curing methods for Ag NP inkjet printed inks. There is no electrical conductivity data in the literature for the same ink-substrate-printer set as used in our study, with oven curing, other than the information on the product data sheet and website [16]. Regarding this information, the sheet resistance obtained with the oven curing in our study matches the one obtained with the same fabrication configuration and curing method by the ink company (7.10^{-6} S/m) and provides validation.

The sheet resistance obtained in our study with the proposed lamination method corresponds to the sheet resistance reported by the company and obtained with

the commercial photonic curing system (pulse-forge), which is claimed to allow curing at higher temperatures without damaging the substrate. While the corresponding conductivity is not reported, on a separate information page the maximum attainable conductivity with photonic curing is given as 33.10^{-6} S/m. Based on these data, we suggest that the proposed lamination curing method (~150\$) provides the same sheet resistance obtained with a much higher initial and technical cost method, photonic curing (~50K\$). Lamination curing saves the curing time dramatically [4, 9, 39] compared to other non-selective thermal curing methods.

Lamination curing method provided a higher electrical conductivity than the self-curing ink and the specially coated PET substrate [5, 6, 40]. Compared with other low glass transition temperature substrate applications, it gave higher conductivity than the plasma curing [9] and was in the range of the conductivities achieved by microwave curing [11]. Other methods are not studied for PET but for high-thermal resistant substrates [9]. We also note that the reported differences in the parameters such as the sample thickness, geometry, nanoparticle size, weight ratio, printing thickness, and measurement methods (number of squares, 4-probe, and 2-probe methods) may avoid an exact comparison between these studies. We note that the laminator company provided the information that the estimated operation range of the laminator was 175 to 215 °C, while we estimated it as 130 to 170 °C. Our thickness estimation of the printed film based on the SEM images is consistent with the thickness reported in [18], using the same ink, substrate, and a similar printer with thermal curing.

A discrepancy between the sheet resistances of the square samples fabricated on different days is detected (Sect. 3.3), for both curing methods. Despite the shift in the magnitudes of the sheet resistances, we emphasize the resistance ratio between the lamination and oven cured samples stayed constant. This indicates the major shift is independent of the curing processes.

4.2.2 Electrical transport mechanism

The printed film and the electrical contacts for the measurements are assumed to exhibit an ohmic behaviour, based on the assumption on the printed films do not exhibit a dielectric regime, but a sufficient percolation [29]. The high conductivity levels we achieve,

Table 6 Lamination curing method provided all the performance criteria defined for the field (See Table 1)

Method	Conductivity	Speed	Film quality	Substrate quality	Cost	Compatibility with R2R	Uncertainty
Lamination	a	d	e	k		n	

Refer to Table 1 for the index explanations

in the same order with the bulk silver (1/4x), rather than levels of magnitude lower conductivities that the metal nanoparticle films exhibit when the percolation is under the sufficient limit ($\sim 10^{-7}$ x) [41], indicates that the diffusion between the metal particles after the curing was adequate to allow conduction by electron percolation through the metallic channels, rather than confining the electrons and the transport mechanism to subtle effects of electron hopping or tunneling [29, 41–43]. This assumption is matching with the information provided in the ink data sheet and similar studies, pointing to the electrical pathways being generated in this range of conductivities [10, 16, 41].

4.2.3 Contact load

While there are several methods that are used to estimate the contact (nip) pressure or load for impression rollers, precise estimation depends on many factors [44–47]. We estimated the contact width and the contact pressure as 1.4 mm and 225 kPa, based on [31] and the contact force measurement. To our knowledge pressure ranges for office-type laminators are not established, however, the value we obtained complies with the range 0–600 kPa which was specified for a pressure-controllable pneumatic laminator [48].

4.3 Suggestions

Regarding the obvious advantages of the lamination curing method in many aspects, we find it worthwhile to inspect the effects of the lamination parameters at wider ranges, with the help of an adjustable laminator (heated roller press) setup. Higher temperatures at higher pressures and speeds or lower roller diameters can be studied, to achieve even more dramatic increases in the curing efficiency, and to define the extent of this combined effect before any damages occur in the samples. It may be also beneficial to study

the improvements in the conductivity around the critical or sub-critical percolation levels altered by the ink and the printing parameters, to further extend the advantages of the method [42].

5 Conclusion

Lamination curing method is found to be a sufficient stand-alone curing method for Ag NP inkjet printed patterns, both on coated and uncoated substrates. It is also found advantageous compared to the conventional oven curing method mainly due to;

- Shorter curing time (80%, 3 mm/s (3 min for an A4 sample)) and warm up time (66%, 5 min),
- Higher nanoparticle aggregation (33% higher conductivity),
- Higher curing temperatures without substrate distortion (applicability on low heat resistant substrates),
- Reduced fabrication uncertainty,
- Higher and more consistent electromechanical sensing performance (of the cured samples).
- Applicability to R2R manufacturing.

When compared to the other curing methods as well, the proposed method provided is found advantageous by providing sufficient performance in all aspects (Table 6). Further inspection can reveal any potential limitation, and how much further the resulting electrical conductivity performance can be improved to compete with the methods like photonic, laser, or electrical curing, however without damaging the thermally sensitive substrates like these methods do. We conclude that the lamination curing for inkjet-printed flexible electronics would accelerate the related prototyping processes by providing a fast, simple, low-cost, and reliable fabrication method addressing the open problems.

Author contributions

All authors contributed to the study conception and design. Material preparation, data collection and analysis were performed by Dila Türkmen. All authors read and approved the final manuscript.

Funding

This work was supported by the Scientific and Technological Research Council of Turkey (TUBITAK) (Grant No. 216M193).

Data availability

The datasets generated during and/or analysed during the current study are available from the corresponding author on reasonable request.

Declarations

Competing interests The authors have no relevant financial or non-financial interests to disclose.

Research involving human and animal rights This research did not contain any studies involving animal or human participants, nor did it take place on any private or protected areas.

Supplementary Information The online version contains supplementary material available at <https://doi.org/10.1007/s10854-023-11220-0>.

References

1. J. Wiklund, A. Karakoç, T. Palko, H. Yiğitler, K. Ruttik, R. Jäntti, J. Paltakari, A review on printed electronics: fabrication methods, inks, substrates, applications and environmental impacts. *J. Manuf. Mater. Process.* **5**(3), 89 (2021)
2. S. Kim, S. Won, G.-D. Sim, I. Park, S.-B. Lee, Tensile characteristics of metal nanoparticle films on flexible polymer substrates for printed electronics applications. *Nanotechnology* **24**(8), 085701 (2013)
3. S. Zhang, L. Cai, W. Li, J. Miao, T. Wang, J. Yeom, N. Sepúlveda, C. Wang, Fully printed silver-nanoparticle-based strain gauges with record high sensitivity. *Adv. Electron. Mater.* **3**(7), 1700067 (2017)
4. B. Ando, S. Baglio, All-inkjet printed strain sensors. *IEEE Sens. J.* **13**(12), 4874–4879 (2013)
5. Y. Kawahara, S. Hodges, B.S. Cook, C. Zhang, G.D. Abowd, Instant inkjet circuits: lab-based inkjet printing to support rapid prototyping of ubicomp devices. in *Proceedings of the 2013 ACM International Joint Conference on Pervasive and Ubiquitous Computing*, 2013, pp. 363–372
6. M.A.M. Asri, N.A. Ramli, A.N. Nordin, Electrical performance and reliability assessment of silver inkjet printed circuits on flexible substrates. *J. Mater. Sci.* 1–14 (2021)
7. S. Wünscher, R. Abbel, J. Perelaer, U.S. Schubert, Progress of alternative sintering approaches of inkjet-printed metal inks and their application for manufacturing of flexible electronic devices. *J. Mater. Chem. C* **2**(48), 10232–10261 (2014)
8. G. Khinda, M. Kokash, M. Alhendi, M. Yadav, J. Lombardi, D. Weerawarne, M.D. Poliks, P. Borgesen, N.C. Stoffel, Effects of oven and laser sintering parameters on the electrical resistance of ijp nano-silver traces on mesoporous pet before and during fatigue cycling. in *2019 IEEE 69th Electronic Components and Technology Conference (ECTC)*, 2019, pp. 1946–1951. IEEE
9. J. Niittynen, R. Abbel, M. Mäntysalo, J. Perelaer, U.S. Schubert, D. Lupo, Alternative sintering methods compared to conventional thermal sintering for inkjet printed silver nanoparticle ink. *Thin Solid Films* **556**, 452–459 (2014)
10. J. Perelaer, P.J. Smith, D. Mager, D. Soltman, S.K. Volkman, V. Subramanian, J.G. Korvink, U.S. Schubert, Printed electronics: the challenges involved in printing devices, interconnects, and contacts based on inorganic materials. *J. Mater. Chem.* **20**(39), 8446–8453 (2010)
11. J. Perelaer, M. Klokkenburg, C.E. Hendriks, U.S. Schubert, Microwave flash sintering of inkjet-printed silver tracks on polymer substrates. *Adv. Mater.* **21**(47), 4830–4834 (2009)
12. P. Escobedo, M.A. Carvajal, J. Banqueri, A. Martínez-Olmos, L.F. Capitán-Vallvey, A.J. Palma, Comparative study of inkjet-printed silver conductive traces with thermal and electrical sintering. *IEEE Access* **7**, 1909–1919 (2018)
13. NovaCentrix Pulse-Forge Photonic Curing System. <https://pulseforge.com/curing-sintering/>. Accessed 9 Apr 2023
14. D. Türkmen, M.A. Kalafat, Improving inkjet printed flexible angle sensor performance by compression-tension sensor pair compensation. *Sens. Actuators A* **345**, 113752 (2022)

15. Z. Zhakypov, J. Paik, Design methodology for constructing multimaterial origami robots and machines. *IEEE Trans. Rob.* **34**(1), 151–165 (2018)
16. Novacentrix, Melaton JS-B25P Nanosilver Ink—Aqueous Dispersion for Dimatix and Epson Printheads. (2016). Novacentrix. <https://www.novacentrix.com/datasheet/Metalon-JS-B25P-TDS.pdf>
17. M. Kim, H. Jee, J. Lee, Photo-sintered silver thin films by a high-power uv-led module for flexible electronic applications. *Nanomaterials* **11**(11), 2840 (2021)
18. E. Gieva, G. Nikolov, B. Nikolova, Sheet resistance measurement of inkjet printed layers. in *2019 42nd International Spring Seminar on Electronics Technology (ISSE)*, pp. 1–6 (2019). <https://doi.org/10.1109/ISSE.2019.8810284>
19. G.S. Khinda, A. Umar, R.J. Cadwell, M. Alhendi, N.C. Stoffel, P. Borgesen, M.D. Poliks, Flexible inkjet-printed patch antenna array on mesoporous pet substrate for 5g applications with stable rf performance after mechanical stress cycling. in *2020 IEEE 70th Electronic Components and Technology Conference (ECTC)*, pp. 1824–1831. IEEE (2020)
20. EPSON, EcoTank L3150. EPSON. https://www.epson.eu/en_EU/products/printers/inkjet/consumer/ecotank-l3150/p/22933. Accessed 13 June 2023
21. Novacentrix, Novele IJ-220. Novacentrix. <https://www.novacentrix.com/datasheet/Novele%20IJ-220.pdf>. Accessed 13 June 2023
22. Mitsubishi Paper Mills Self Curing Silver Ink. <https://www.mpm.co.jp/electronic/eng/silver-nano/faq.html>. Accessed 10 Apr 2023
23. Sigma-Aldrich, Product Specification 736465. Sigma-Aldrich. https://www.sigmaaldrich.com/specification-sheets/202/456/736465-BULK_ALDRICH_.pdf. Accessed 13 June 2023
24. un55. <https://www.memmert.com/products/heating-drying-ovens/universal-oven/UN55/>. Accessed 7 August 2023
25. OLYMPIA, Laminator A3048. OLYMPIA. https://www.olympia-vertrieb.de/fileadmin/produkte/laminiergeraete/A2024_A2048_A3024_A3048_User_Manual_20200227.pdf. Accessed 15 June 2023
26. DF Robot, Thin Film Pressure Sensor RP-L-170. DF Robot. <https://www.dfrobot.com/product-1843.html>. Accessed 15 June 2023
27. J. Pütz, S. Heusing, M. Aegerter, Characterization of electrical properties. in *Handbook of Sol-Gel Science and Technology*, ed. by L. Klein, M. Aparicio, A. Jitianu, 2005, pp. 1–30
28. I. Miccoli, F. Edler, H. Pfnür, C. Tegenkamp, The 100th anniversary of the four-point probe technique: the role of probe geometries in isotropic and anisotropic systems. *J. Phys.* **27**(22), 223201 (2015)
29. P. Sheng, Electronic transport in granular metal films. in *Nanophase Materials: Synthesis—Properties—Applications*, 1994, pp. 381–398
30. Y. Lu, P.R. Pagilla, Modeling of temperature distribution in moving webs in roll-to-roll manufacturing. *J. Therm. Sci. Eng. Appl.* **6**(4), 041012 (2014)
31. H. Chu, Q. Yu, C. Zhang, Q. Chen, R. Ding, Y. Hong, Contact characteristics of steel-rubber rollers based on modified contact theory considering viscoelasticity. *Proc. Inst. Mech. Eng. C J. Mech. Eng. Sci.* **236**(1), 456–470 (2022)
32. T.S. Wiśniewski, P. Furmanski, Thermal contact resistance, in *Encyclopedia of Thermal Stresses*. ed. by R.B. Hetnarski (Springer, Dordrecht, 2014), pp.4957–4968. <https://doi.org/10.1007/978-94-007-2739-7>
33. J.J. Fuller, E. Marotta, Thermal contact conductance of metal/polymer joints: an analytical and experimental investigation. *J. Thermophys. Heat Transf.* **15**(2), 228–238 (2001)
34. T. Zhou, Y. Zhao, Z. Rao, Fundamental and estimation of thermal contact resistance between polymer matrix composites: a review. *Int. J. Heat Mass Transf.* **189**, 122701 (2022)
35. A. Hussain, H.-L. Lee, Y.-J. Moon, H. Kang, S.-J. Moon, J.-Y. Hwang, Temperature estimation during pulsed laser sintering of silver nanoparticles. *Appl. Sci.* **12**(7), 3467 (2022)
36. J. Wojtkowiak, Lumped thermal capacity model. *Encycl. Therm. Stresses* 2808–2817 (2014)
37. Memmert Operating Instructions. <https://www.memmert.com/index.php?eID=dumpFile &t=f &f=3893 &token=25ec4464160111af0674233631f1b0d0ecdcc5d0>. Accessed 10 August 2023
38. Pinch Rollers, Pressure Measurement. <https://www.sensorprod.com/glossary/pinch-roller/pinch-rollers.php>. Accessed 10 August 2023
39. M.A. Riheen, T.K. Saha, P.K. Sekhar, Inkjet printing on pet substrate. *J. Electrochem. Soc.* **166**(9), 3036 (2019)
40. C. Beisteiner, R. Gstöttenmayr, T. Altmanninger, B.G. Zagar, Charakterisierung von mechanischen und elektrischen eigenschaften funktionaler inkjet-gedruckter strukturen: tm -. *Tech. Mess.* **83**(11), 647–659 (2016). <https://doi.org/10.1515/teme-2016-0017>
41. J. Leppäniemi, T. Mattila, T. Kololuoma, M. Suhonen, A. Alastalo, Roll-to-roll printed resistive worm memory on a flexible substrate. *Nanotechnology* **23**(30), 305204 (2012)
42. C.B. Van den Berg, et al., Structural and electrical characteristics of printed metal nanoparticle networks. Master's thesis, University of Cape Town (2016)

43. A. Kavokin, S. Kutrovskaya, A. Kucherik, A. Osipov, T. Vartanyan, S. Arakelyan, The crossover between tunnel and hopping conductivity in granulated films of noble metals. *Superlatt. Microstruct.* **111**, 335–339 (2017)
44. L. Yang, Printing dynamics: Nip pressure and its relationship with materials' viscoelasticity. *J. Packag. Technol. Res.* **4**(2), 145–156 (2020)
45. G. Bindhumadhavan, J. Seville, M. Adams, R. Greenwood, S. Fitzpatrick, Roll compaction of a pharmaceutical excipient: experimental validation of rolling theory for granular solids. *Chem. Eng. Sci.* **60**(14), 3891–3897 (2005)
46. Fujifilm, PRESCALE / THERMOSCALE / UVSCALE. Fujifilm. <https://www.fujifilm.com/ca/en/business/industrial-materials/measurement-film/prescale/download>
47. K.N. Bachus, A.L. DeMarco, K.T. Judd, D.S. Horwitz, D.S. Brodke, Measuring contact area, force, and pressure for bioengineering applications: using fuji film and tekscan systems. *Med. Eng. Phys.* **28**(5), 483–488 (2006)
48. ICO, HA Series Laminating. ICO. <http://www.ico-deli.com/en/?c=p &a=canpinxq &myid= &zid=15 &id=31>

Publisher's Note Springer Nature remains neutral with regard to jurisdictional claims in published maps and institutional affiliations.

Springer Nature or its licensor (e.g. a society or other partner) holds exclusive rights to this article under a publishing agreement with the author(s) or other rightsholder(s); author self-archiving of the accepted manuscript version of this article is solely governed by the terms of such publishing agreement and applicable law.